

## ON THE HIGH-FREQUENCY QUASI-PERIODIC OSCILLATIONS FROM BLACK HOLES

M. HAKAN ERKUT

Department of Physics, İstanbul Kültür University, Ataköy Campus, Bakırköy 34156, İstanbul, Turkey

## ABSTRACT

We apply the global mode analysis, which has been recently developed for the modeling of kHz quasi-periodic oscillations (QPOs) from neutron stars, to the inner region of an accretion disk around a rotating black hole. Within a pseudo-Newtonian approach that keeps the ratio of the radial epicyclic frequency  $\kappa$  to the orbital frequency  $\Omega$  the same as the corresponding ratio for a Kerr black hole we determine the innermost disk region where the hydrodynamic modes grow in amplitude. We find that the radiation flux emerging from the inner disk has the highest values within the same region. Using the flux weighted averages of the frequency bands over this region we identify the growing modes with highest frequency branches  $\Omega + \kappa$  and  $\Omega$  to be the plausible candidates for the high-frequency QPO pairs observed in black hole systems. The observed frequency ratio around 1.5 can therefore be understood naturally in terms of the global free oscillations in the innermost region of a viscous accretion disk around a black hole without invoking a particular resonance to produce black hole QPOs. Although the frequency ratio  $\langle \Omega + \kappa \rangle / \langle \Omega \rangle$  is found to be not sensitive to the black hole's spin which is good for explaining the high-frequency QPOs it may work as a limited diagnostic of the spin parameter to distinguish black holes with very large spin from the slowly rotating ones. Within our model we estimate the frequency ratio of a high-frequency QPO pair to be greater than 1.5 if the black hole is a slow rotator. For fast rotating black holes, we expect the same ratio to be less than 1.5.

*Keywords:* accretion, accretion disks — black hole physics — stars: oscillations — X-rays: stars

## 1. INTRODUCTION

The high energy emission from neutron stars and black holes in X-ray binaries is generally powered by accretion onto the compact object. The variability of X-ray light curve with different time scales from milliseconds to days is usually attributed to various characteristic time scales associated with accretion flow around the black hole or neutron star. In low-mass X-ray binaries (LMXBs), where the central object is fed by an accretion disk, a few variability frequencies observed as quasi-periodic oscillation (QPO) peaks in addition to other broad-band features in the power spectra are common to both black hole and neutron star sources. Although there are some phenomenological differences between QPOs in black hole candidates and those observed in neutron star LMXBs, the similarities such as tight correlations of high and low frequency power spectral features in black hole and neutron star sources are remarkable (van der Klis 1994; Psaltis, Belloni, & van der Klis 1999; Wijnands & van der Klis 1999). Any interpretation or model solely based on the existence of a magnetic field, a hard surface, which are neutron star like properties, or an innermost stable circular orbit (ISCO) as a black hole like property to produce QPOs cannot account for the correlations of timing properties among different sources.

QPOs were discovered in the X-ray power density spectrum of black hole transients with frequencies in the  $\approx 0.1 - 360$  Hz range during the very high spectral state of these sources (Motch et al. 1983; Miyamoto & Kitamoto 1989; Miyamoto et al. 1991; Morgan, Remillard, & Greiner 1997; Wijnands, Homan, & van der Klis 1999; Sobczak et al. 2000; Strohmayer 2001; Muno et al. 2001). For several black hole sources, high-frequency QPOs were observed as single peaks roughly around 200 Hz (see Remillard & McClintock 2006 and references therein). The discovery of twin kHz QPOs in neutron star LMXBs with their peak frequencies within around the 200 – 1200 Hz range and a peak separation in the

$\approx 180 - 360$  Hz range together with their tight correlations with the low frequency power spectral components which are also observed in black hole candidates strengthens the idea that QPOs are produced in the inner regions of accretion disks around compact objects (see van der Klis 2000 and references therein; Méndez & Belloni 2007). The discoveries of twin hectoHz QPOs from black hole candidates such as GRO J1655–40, XTE J1550–564, and GRS 1915+105 (Remillard et al. 2002, 2003; Remillard & McClintock 2006) have almost certified the idea of unifying the interpretation of high-frequency QPOs observed in black hole and neutron star sources within a single QPO model.

One of the most striking differences between the high-frequency QPOs of black holes and the kHz QPOs in neutron star LMXBs is the fact that the former do not show any significant correlation with the X-ray luminosity whereas the latter do. From one observation to another in a given source, the frequency shifts in the high-frequency QPOs of black holes are negligible as compared to the variations in the frequencies of kHz QPO peaks of accreting neutron stars. As compared to kHz QPOs detected in the power spectra of neutron stars, high-frequency QPOs from black holes are weak features having relatively low-quality factors. The commonly observed property of both low and high-frequency QPOs in black holes is the fact that these oscillations are strongest at photon energies above 6 keV when the power law component in the energy spectra dominates over the disk component (Remillard & McClintock 2006). Though it is not conclusive regarding the number of black hole sources exhibiting twin QPOs, the frequency ratio of the upper high-frequency QPO to the lower one is close to 3:2 in black hole candidates. There is no specific value for the ratio of two simultaneous kHz QPOs observed in neutron star sources; the ratio of the upper QPO frequency to the lower one rather takes different values changing between one and three from one source to another (Belloni, Méndez, & Homan 2005). Beside similarities and tight correlations, the phenomenological differences

between the high-frequency QPOs observed from black hole candidates and those from neutron star LMXBs likely arise from the dominant effect of different boundary conditions imposed by a hard surface or a magnetic field and the ISCO as they might be more appropriate for a neutron star and a black hole, respectively.

High-frequency QPOs were detected in seven black hole sources among which three black hole candidates exhibited QPO pairs in their power spectra. In all the sources with QPO pairs of commensurate frequencies, the ratio of two QPO frequencies is very close to 1.5 in two black hole binaries and to 1.6 in the third one (Remillard et al. 2002; Remillard et al. 2003). The common property of high-frequency QPOs observed in black hole systems is based on the spectral state of a given source. All high-frequency black-hole QPOs are usually observed in very high and high spectral states which are characterized by the most luminous states of the source (see Remillard & McClintock 2006 and references therein). For such high luminosities, the accretion disk around the black hole is expected to be truncated at the radius of the ISCO according to the standard model (Novikov & Thorne 1973; Shakura & Sunyaev 1973). For radii less than the radius of the ISCO, the accreting gas is thought to plunge radially towards the black hole. In the recent MHD simulations by Beckwith, Hawley, & Krolik (2008), however, the innermost ring of the disk which emits significant radiation has been shown to lie inside where the standard model predicts. These simulations have modified the stress-free boundary condition of the standard model at the ISCO, but they have employed the classical relationship between magnetic stresses and energy dissipation and the assumption that the radial inflow time-scale of the accreting matter inside the ISCO is longer than the time-scales for thermalization and radiation of the dissipated heat, both of which may not be valid at all within the plunging region. We therefore anticipate the innermost part of the disk beyond the ISCO to be the most probable region near the black hole for the production of high-frequency QPOs. It is very likely within this region that the frequencies of the unstable growing disk modes correspond to the frequency bands of QPOs.

The early attempts to interpret QPO frequencies in terms of disk modes were made by Alpar et al. (1992) and Alpar & Yilmaz (1997). The initial contributions to the theory of disk oscillations explored the role of trapped disk oscillations in the variability of the X-ray power spectra of black hole sources (Kato & Fukue 1980; Nowak & Wagoner 1991; Kato 2001 and references therein). The general relativistic test-particle frequencies were recognized and employed to construct models of QPOs for both neutron stars and black holes (Stella, Vietri, & Morsink 1999; Abramowicz et al. 2003). The model of Psaltis & Norman (2000) revealed the importance of hydrodynamic corrections to relativistic test-particle frequencies and the effect of hydrodynamic disk parameters on the correlations of QPOs and broad-band noise component. Alpar & Psaltis (2008) noted that the radial epicyclic frequency would be the highest dynamical frequency in the inner region of an accretion disk. This conclusion is based upon the existence of a magnetohydrodynamic boundary region around the neutron star where orbital frequencies deviate from Keplerian test-particle frequencies due to viscous and magnetic stresses (see Erkut & Alpar 2004). The recent analysis by Erkut, Psaltis, & Alpar (2008) of global hydrodynamic modes in the boundary regions of neutron stars showed how important the hydrodynamic effects are in estimating the observational characteristics of high-frequency QPOs.

In this paper we apply the mode analysis, which has been developed by Erkut, Psaltis, & Alpar (2008) for the boundary region model of kHz QPOs from neutron stars, to the inner region of an accretion disk around a Kerr black hole. In order to account for the general relativistic effects of a Kerr metric on the ratio of dynamical frequencies, we work with a new pseudo-Newtonian potential that is appropriate for the analysis of temporal behavior of relativistic disks. This approach allows us to extend our recent study of global hydrodynamic modes of free oscillations to black holes as well. Our aim is to identify the modes whose frequency bands correspond to the high-frequency QPO pairs usually detected with a frequency ratio close to 1.5 in black hole sources. Most importantly, we provide a way to use the frequency ratio of these modes as a diagnostics of the spin parameter of a rotating black hole that exhibit high-frequency QPOs.

In Section 2 we introduce our pseudo-Newtonian approach. The basic equations and parameters related to the analysis of disk modes for a Kerr black hole are presented in Section 3. In Section 4 we come up with the mode analysis and identify the modes relevant to the commensurate high-frequency QPO pairs with a frequency ratio around 1.5. We discuss the results and present our conclusions in Section 5.

## 2. PSEUDO-NEWTONIAN TREATMENT OF FREQUENCIES

Using pseudo-Newtonian potentials in hydrodynamic simulations is an effective and easy method to incorporate relativistic effects into accretion flows (e.g., Chan, Psaltis, & Özel 2009). The pseudo-Newtonian potential proposed by Paczyński & Wiita (1980) is successful in estimating the ISCO for Schwarzschild geometry. It is therefore appropriate for a non-rotating black hole. Recently, two modified Newtonian force models have been introduced by Mukhopadhyay & Misra (2003) to approximate the dynamical frequencies of an accretion disk around a rotating black hole.

In our current analysis, the ratio of two successive frequency bands of disk modes is of interest in identifying the high-frequency QPOs from black holes. Unlike the early studies we mentioned above our pseudo-Newtonian treatment of dynamical disk frequencies keeps the ratio of the radial epicyclic frequency  $\kappa$  to the orbital frequency  $\Omega$  exactly the same as the corresponding ratio observed by a distant observer of a Kerr black hole.

The Kerr expression for the ratio of the test-particle frequencies  $\kappa$  and  $\Omega$  is

$$\frac{\kappa}{\Omega} = \sqrt{1 - 6 \left( \frac{R_g}{r} \right) + 8a \left( \frac{R_g}{r} \right)^{3/2} - 3a^2 \left( \frac{R_g}{r} \right)^2}, \quad (1)$$

where  $a$  is the spin parameter of the black hole and  $R_g = GM/c^2$  with  $M$  and  $c$  being the mass of the black hole and the speed of light, respectively. The Newtonian expression for the same ratio is

$$\frac{\kappa}{\Omega} = \sqrt{2 \left( 2 + \frac{d \ln \Omega}{d \ln r} \right)}. \quad (2)$$

The ratio given by equation (2) is valid for both the test-particles and the hydrodynamical fluids rotating in orbits. In the steady state of a geometrically thin disk, the hydrodynamical effects of pressure gradients on the test-particle frequencies are negligible. As we mention in Section 3, the radial momentum balance in a geometrically thin disk can be approximated by the test-particle orbits where the centripetal ac-

celeration of each gas particle rotating with the frequency  $\Omega$  is due to the gravitational force. Setting equations (1) and (2) equal to each other, we obtain within our pseudo-Newtonian approach a differential equation for the orbital frequency  $\Omega(r)$ . Given a suitable pseudo-Newtonian potential, the orbital frequency  $\Omega$  satisfies the radial momentum equation and mimics the effect of strong gravity on the gas-particle orbits by keeping the value of  $\kappa/\Omega$  the same as the corresponding Kerr value in the test-particle regime. In this sense, our approach is similar to the early pseudo-Newtonian treatments of the dynamical frequencies in a geometrically thin accretion disk around a black hole. To find a solution for  $\Omega(r)$ , we require that our pseudo-Newtonian orbital frequency match the Kerr orbital frequency in the outer disk. According to a distant observer, the Kerr expression for the orbital frequency is

$$\Omega_{\text{Kerr}}(r) = \frac{\Omega_{\text{K}}(r)}{1 + a \left( R_{\text{g}}/r \right)^{3/2}}, \quad (3)$$

where  $\Omega_{\text{K}}(r) = (GM/r^3)^{1/2}$  is the Keplerian frequency. For sufficiently large radii, that is for  $r \gg R_{\text{g}}$ , the Kerr orbital frequency assumes its Keplerian value. Using the same asymptotic boundary condition on the pseudo-Newtonian orbital frequency, it follows from equations (1) and (2) that

$$\Omega(r) = \Omega_{\text{K}}(r) \exp \left[ 3 \left( \frac{R_{\text{g}}}{r} \right) - \frac{8}{3} a \left( \frac{R_{\text{g}}}{r} \right)^{3/2} + \frac{3}{4} a^2 \left( \frac{R_{\text{g}}}{r} \right)^2 \right]. \quad (4)$$

To illustrate our treatment of the radial epicyclic and orbital frequencies, we plot in Figure 1 the pseudo-Newtonian frequencies  $\kappa$  and  $\Omega$  over a wide range of disk radii in comparison with the corresponding Kerr frequencies. Figure 1a shows the radial profiles of  $\kappa$  and  $\Omega$  for a Schwarzschild black hole for which the spin parameter  $a = 0$ . The radial profiles of the same frequencies for a Kerr black hole with a spin parameter  $a = 0.8$  are shown in Figure 1b. The pseudo-Newtonian frequencies  $\kappa$  and  $\Omega$  can be seen to slightly deviate from the Kerr frequencies in the inner disk while they asymptotically match them in the outer disk. Note, however, that the pseudo-Newtonian frequency  $\kappa$  always yields the correct estimation for the ISCO as  $\kappa/\Omega$  matches its Kerr value exactly for all disk radii.

In the next section, we present the basic equations for a geometrically thin disk and obtain within the current pseudo-Newtonian approach the hydrodynamic parameters that are necessary for the analysis of global modes in the inner disk.

### 3. BASIC EQUATIONS AND PARAMETERS

The long-wavelength global hydrodynamic modes of free oscillations have been recently studied for the boundary regions of accretion disks around neutron stars (see Erkut, Psaltis, & Alpar 2008, hereafter EPA08). In the mode analysis by EPA08 the basic disk equations are perturbed for a geometrically thin disk in vertical hydrostatic equilibrium. The Fourier decomposition of the linearized perturbation equations leads to the identification of the complex mode frequencies  $\omega^{(m)}$ . The real parts of axisymmetric ( $m = 0$ ) and nonaxisymmetric ( $m \geq 1$ ) mode frequencies correspond to the frequency bands of QPOs while the imaginary parts determine the growth rates of the oscillations.

In the global mode analysis, both the frequency bands and their growth rates depend on several key parameters such as  $\kappa/\Omega$ , the radial profile of the surface density,  $\beta$ , the inverse

timescale  $\Omega_{\nu}$  associated with the radial drift velocity, and the inverse timescale  $\Omega_s$  associated with the sound speed in the inner disk. These parameters are determined by the global structure of the unperturbed steady disk (see EPA08).

For sufficiently high mass accretion rates, e.g.,  $\dot{M} \gtrsim 0.1 \dot{M}_{\text{E}}$ , where  $\dot{M}_{\text{E}}$  is the Eddington mass accretion rate, black holes in LMXBs accrete matter through radiatively efficient accretion disks whose innermost regions are dominated by radiation pressure (Shakura & Sunyaev 1973, hereafter SS73). The innermost truncation radius of such a disk around a Kerr black hole is estimated by the radius of the ISCO,  $r_{\text{in}}$ , which can be found as a solution of  $\kappa/\Omega = 0$  for  $r = r_{\text{in}}$  (see eq. [1]). The unperturbed steady structure of a radiation pressure dominated inner disk is described by

$$\rho c_s^2 = \frac{\varepsilon}{3}, \quad (5)$$

where  $c_s$  is the effective sound speed,  $\rho$  is the average mass density, and  $\varepsilon$  is the radiation energy density. We write, for the vertical hydrostatic equilibrium in the disk,

$$c_s^2 = \frac{1}{2} \Omega^2 H^2, \quad (6)$$

where  $H$  is the half-thickness of the disk. The average mass density can be expressed in terms of the surface mass density  $\Sigma$  as

$$\rho = \frac{\Sigma}{2H}. \quad (7)$$

The vertical energy balance in the inner disk is satisfied for

$$\varepsilon = \left( \frac{3\kappa_{\text{es}}\Sigma}{4c} \right) \Phi, \quad (8)$$

where  $\kappa_{\text{es}}$  is the electron scattering opacity and  $\Phi$  is the energy dissipation rate per unit area of the disk (see SS73). The energy flux due to viscous energy dissipation is

$$\Phi = \frac{1}{2} \nu \Sigma \left( r \frac{d\Omega}{dr} \right)^2. \quad (9)$$

Here,  $\nu$  is the kinematic viscosity for which the  $\alpha$ -prescription (SS73) can be written as

$$-\alpha \Sigma c_s^2 = \nu \Sigma r \frac{d\Omega}{dr}. \quad (10)$$

For a geometrically thin disk, the radial momentum balance can be written to a good approximation as  $\Omega^2 r - d\Gamma/dr = 0$ , where  $\Gamma$  is the pseudo-Newtonian potential that mimics the gravitational field of the black hole. In the radial momentum equation, the pseudo-Newtonian force,  $-d\Gamma/dr$ , is the source of acceleration,  $-\Omega^2 r$ , where  $\Omega$  is given by equation (4). For the conservation of mass and angular momentum, we write

$$-2\pi r \Sigma v_r = \dot{M} \quad (11)$$

and

$$2\pi \nu \Sigma r^3 \frac{d\Omega}{dr} + \dot{M} r^2 \Omega = C, \quad (12)$$

respectively, where  $v_r$  is the radial drift velocity of the accreting matter in the inner disk and  $C$  is an arbitrary constant of integration.

We solve equation (12) using torque-free boundary condition at the innermost disk radius,  $r_{\text{in}}$ , which is appropriate for a disk around a black hole. The constant of integration can be

determined as  $C = \dot{M} r_{\text{in}}^2 \Omega(r_{\text{in}})$  to satisfy the torque-free boundary condition. Using equation (4), it follows from equations (5)–(12) that

$$\beta \equiv \frac{d \ln \Sigma}{d \ln r} = \frac{3}{2} - B(r) - \frac{D(r)}{A(r)} - \frac{E(r)}{F(r)}, \quad (13)$$

$$\frac{\Omega_\nu}{\Omega_s} \equiv -\frac{v_r/r}{c_s/r} \simeq 2.57 \alpha \dot{m} \left( \frac{6R_g}{r} \right) A(r), \quad (14)$$

$$\frac{\Omega_s}{\Omega} \simeq 2.4 \dot{m} \left( \frac{6R_g}{r} \right) A(r) F(r), \quad (15)$$

and

$$\frac{\Phi}{\Phi_t} = \left( \frac{r}{r_{\text{in}}} \right)^{-3} f^2(r) A(r) F(r), \quad (16)$$

where  $\Phi_t \equiv 3GM\dot{M}/8\pi r_{\text{in}}^3$  is the typical value for the radiation flux and

$$\dot{m} \equiv \frac{\dot{M}}{\dot{M}_E} = \frac{\dot{M}}{1.9 \times 10^{18} \text{g s}^{-1}} \left( \frac{\eta}{0.06} \right) \left( \frac{M}{M_\odot} \right)^{-1}. \quad (17)$$

Here,  $\eta$  is a function of the spin parameter  $a$  such that

$$a = \frac{4\sqrt{2} [1 - (1 - \eta)^2]^{1/2} - 2(1 - \eta)}{3\sqrt{3} [1 - (1 - \eta)^2]} \quad (18)$$

for prograde accretion disks around rotating black holes (see Shapiro & Teukolsky 1983). In equations (13)–(16), the dimensionless factors arising from the boundary conditions and pseudo-Newtonian corrections are

$$A(r) = 1 + 2 \left( \frac{R_g}{r} \right) - \frac{8}{3} a \left( \frac{R_g}{r} \right)^{3/2} + a^2 \left( \frac{R_g}{r} \right)^2, \quad (19)$$

$$B(r) = -3 \left( \frac{R_g}{r} \right) + 4a \left( \frac{R_g}{r} \right)^{3/2} - \frac{3}{2} a^2 \left( \frac{R_g}{r} \right)^2, \quad (20)$$

$$D(r) = -4 \left( \frac{R_g}{r} \right) + 8a \left( \frac{R_g}{r} \right)^{3/2} - 4a^2 \left( \frac{R_g}{r} \right)^2, \quad (21)$$

$$E(r) = \frac{f(r_{\text{in}})}{f(r)} \left( B(r) + \frac{1}{2} \right) \left( \frac{r}{r_{\text{in}}} \right)^{-1/2}, \quad (22)$$

and

$$F(r) = 1 - \frac{f(r_{\text{in}})}{f(r)} \left( \frac{r}{r_{\text{in}}} \right)^{-1/2}, \quad (23)$$

with

$$f(r) = \exp \left[ 3 \left( \frac{R_g}{r} \right) - \frac{8}{3} a \left( \frac{R_g}{r} \right)^{3/2} + \frac{3}{4} a^2 \left( \frac{R_g}{r} \right)^2 \right]. \quad (24)$$

For illustrative purposes we display in Figure 2 the radial distributions of the outgoing radiation flux (see eq. [16]) throughout the inner disk for two putative black holes with spin parameters  $a = 0$  and  $a = 0.9$ . In the following section, we use the ratio  $\kappa/\Omega$  (see eq. [1]) and the global hydrodynamic parameters  $\beta$ ,  $\Omega_\nu/\Omega_s$ , and  $\Omega_s/\Omega$  (see eq. [13]–[15]) to identify the radial zone in the inner disk where the modes grow. As we will see, the hydrodynamic modes grow only within a limited range of radii in the innermost disk region out of which the radiation flux is maximum (see Fig. 2).

#### 4. GLOBAL MODES IN THE INNER DISK

When there are no external perturbations due to large-scale magnetic fields of the accreting star, the free oscillation modes in a boundary region or the inner disk are excited through the dynamical effect of the viscosity. In the limit of small hydrodynamic corrections, this can be seen from the growth rates of both axisymmetric and nonaxisymmetric modes for which  $\text{Im}(\omega^{(m)}) \propto -\beta\Omega_\nu$  (see EPA08). In the presence of viscosity and therefore of radial drift velocity,  $\Omega_\nu \neq 0$  and the high-frequency modes can have positive growth rates only if  $\beta < 0$ . This is also valid for the global modes in a disk around a black hole. Unlike neutron stars, the effect of a large-scale toroidal magnetic force in addition to viscosity on the excitation of global modes might be absent in the case of black holes (see Section 3 in EPA08).

For a black hole disk, the presence of the ISCO with a torque-free boundary condition determines the radial profile of the surface density,  $\beta$ , and thus the growth rates of the modes. Note that  $\beta \simeq 3/2 > 0$  for  $r \gg r_{\text{in}}$  (see eq. [13]) and we expect, in the regime of small hydrodynamic corrections, that the global hydrodynamic modes do not grow for sufficiently large radii in the inner disk. For the innermost disk region, however, the hydrodynamic corrections can be important to distinguish among the growth rates of different modes and to identify the set of radii at which these modes grow. In order to see the effects of hydrodynamic parameters on both the frequency bands and growth rates of the modes in the inner disk beyond the regime of negligible hydrodynamic corrections, we use equations (13)–(15) together with equation (1) in the full eigenfrequency solutions for axisymmetric and nonaxisymmetric perturbations given in the Appendix of EPA08.

Figures 3–6 show the real and imaginary parts of the complex mode frequencies in units of the orbital frequency  $\Omega$  as functions of the radial distance in the inner disk. The real and imaginary parts represent the frequency bands and the growth rates of the modes, respectively. In Figures 3–6, we label the hydrodynamic mode frequencies and their growth rates with notation corresponding to the test-particle frequencies. This provides us with an easy identification and a simple designation of each mode without ambiguity and without loss of generality. In the limit of small hydrodynamic corrections, the frequencies of all hydrodynamic modes converge to the test-particle frequencies. We mark axisymmetric ( $m = 0$ ) modes with the corresponding test-particle frequencies  $\omega = 0$  and  $\omega = \kappa$ . We use  $\omega = \Omega$  and  $\omega = \Omega \pm \kappa$  as the appropriate labels to distinguish among nonaxisymmetric modes ( $m = 1$ ).

Figure 3a exhibits the run of the mode frequencies in the inner disk of a Schwarzschild black hole ( $a = 0$ ). We display the growth rates of the modes in Figure 3b. Figure 3 is obtained for  $\alpha = 0.1$  and  $\dot{m} = 0.1$ . Note that the hydrodynamic modes do not grow in the inner disk for  $r \gtrsim 2.3r_{\text{in}}$ . The radial zone within which all modes grow covers only a limited range of radii around  $r_{\text{in}} - 2.1r_{\text{in}}$  in the innermost disk region, as shown in Figure 3b. The hydrodynamic modes with frequency bands around  $\Omega$  and 0 have relatively higher growth rates as compared to those around  $\Omega \pm \kappa$  and  $\kappa$  bands. Figure 4 reveals how the mode frequencies and the growth rates are affected by the rotation of the black hole. For the same values of the viscosity parameter and the mass accretion rate, that is, for  $\alpha = 0.1$  and  $\dot{m} = 0.1$ , we plot the frequency profiles of the modes in Figure 4a and the corresponding growth rates in Figure 4b for a rotating black hole with a spin parameter

$a = 0.9$ . In comparison with Figure 3b, the growth rates of the modes are higher in Figure 4b. The range of radii at which the hydrodynamic modes grow is around  $r_{\text{in}} - 2.3r_{\text{in}}$ . All modes decay for  $r \gtrsim 2.5r_{\text{in}}$  (see Fig. 4b). We obtain Figure 5 and Figure 6 keeping the spin parameter of the black hole at  $a = 0.9$ , however, changing the viscosity parameter  $\alpha$  and the mass accretion rate  $\dot{m}$ . For  $\alpha = 0.01$  and  $\dot{m} = 0.1$ , we explore the run of the mode frequencies and the growth rates in Figures 5a and 5b, respectively. As compared to Figure 4a, the radial profiles of the mode frequencies can be seen to be almost unaffected by a change in the viscosity parameter  $\alpha$  (see Fig. 5a). We observe, in Figure 5b, that the growth rates are lower than those in Figure 4b by a factor around 0.1 which, indeed, is the factor of decrease in  $\alpha$ . Figure 6 is obtained for  $\dot{m} = 0.6$  while keeping the values of  $\alpha$  and the spin parameter  $a$  the same as in Figure 5. Note that both the frequency bands and the growth rates of the modes are modified to some level at relatively high mass accretion rates. The greater the mass accretion rate  $\dot{m}$ , the higher are the growth rates of hydrodynamic modes (see Fig. 6b). We note that the frequency bands that are related to  $\Omega \pm \kappa$ ,  $\Omega$ , and  $\kappa$  branches in the limit of small hydrodynamic corrections begin to deviate from the test-particle frequencies for sufficiently large mass accretion rates ( $\dot{m} \gtrsim 0.6$ ) as shown in Figure 6a.

The common property of Figures 3–6 is that all the hydrodynamic modes grow within a limited region in the innermost part of the disk with characteristic radii in the  $\simeq r_{\text{in}} - 2.5r_{\text{in}}$  range. The radiation flux emerging from the same region attains the highest values with maxima at  $r \simeq 1.6r_{\text{in}}$  and  $r \simeq 1.7r_{\text{in}}$  for the black holes with spin parameters  $a = 0$  and  $a = 0.9$ , respectively (see Fig. 2). It is interesting to deduce from Figures 3–6 that the frequency ratio of the hydrodynamic modes we associate with  $\Omega + \kappa$  and  $\Omega$  frequency bands is close to 1.5 at radii in the  $\simeq (1.6 - 1.7)r_{\text{in}}$  range, where the disk flux is maximum. As mentioned above, the modes, however, grow throughout an extended region, with  $r_{\text{in}} < r < 2.5r_{\text{in}}$ , of radii rather than being excited at a particular radius. Moreover, the modes with frequencies around  $\Omega - \kappa$  and  $\kappa$  bands also grow within the same region. To distinguish among the pairs of growing modes which can be regarded as plausible candidates for the high-frequency QPO pairs from black holes, we consider the mutual ratios of the flux weighted averages of the frequency bands for different modes. We define the flux weighted average of a frequency branch  $\omega$  as

$$\langle \omega \rangle = \int_{r_{\text{in}}}^{r_c} 2\pi r \omega(r) \Phi(r) dr \Big/ \int_{r_{\text{in}}}^{r_c} 2\pi r \Phi(r) dr, \quad (25)$$

where  $r_c$  is the critical radius beyond which the corresponding mode decays in the inner disk. Using equation (25), we calculate the ratios of the flux weighted averages of the frequency bands  $\Omega + \kappa$ ,  $\Omega$ ,  $\Omega - \kappa$ , and  $\kappa$  for different values of the black hole spin parameter  $a$  between 0 and 1. For each model value of  $a$ , we find a critical radius  $r_c$  such that all the hydrodynamic modes grow for  $r \leq r_c$ . Unlike the growth rates, the mode frequencies and the width of the radial zone where the modes grow are sensitive to the spin parameter  $a$ , but not sensitive to the viscosity parameter  $\alpha$  and the mass accretion rate  $\dot{m}$  (see Figs. 3–6). In Figure 7 we display the run of  $\langle \Omega + \kappa \rangle / \langle \Omega \rangle$ ,  $\langle \Omega \rangle / \langle \kappa \rangle$ , and  $\langle \Omega \rangle / \langle \Omega - \kappa \rangle$  for  $0 \leq a \lesssim 1$ . Figure 7 is obtained for the typical values,  $\alpha = 0.1$  and  $\dot{m} = 0.1$ . The values for  $\langle \Omega + \kappa \rangle / \langle \Omega \rangle$  are densely clustered around 1.5 over a wide range of values for  $a$  as shown in Figure 7. For slow rotators ( $a \simeq 0$ ),  $\langle \Omega + \kappa \rangle / \langle \Omega \rangle \simeq 1.6$ . The same ratio drops below

1.5 as  $a$  approaches 1 for rapidly rotating black holes. The values of  $\langle \Omega \rangle / \langle \kappa \rangle$  and  $\langle \Omega \rangle / \langle \Omega - \kappa \rangle$ , on the other hand, span a wide range as the spin parameter  $a$  varies between 0 and 1 (see Fig. 7). Our analysis suggests the hydrodynamic modes with frequency bands around  $\Omega + \kappa$  and  $\Omega$  to be the plausible candidates for the high-frequency QPO pairs observed in black hole systems. Note that our model estimation for the frequency ratio of high-frequency QPO pairs involves the two highest frequency modes with positive growth rates.

We give examples for surface density perturbations of such global modes in Figures 8–11. We display the three dimensional profile of surface density perturbation  $\Sigma_1$  in terms of background surface density  $\Sigma_0$  in the innermost region ( $r_{\text{in}} \leq r \leq 3r_{\text{in}}$ ) of a disk around a rotating black hole with spin parameter  $a = 0.9$  for the typical values,  $\alpha = 0.1$  and  $\dot{m} = 0.1$ . The examples for nonaxisymmetric modes with frequencies  $\Omega$  (Fig. 8) and  $\Omega + \kappa$  (Fig. 9) show the surface density perturbations at the time  $t = 2P_{\text{in}}$ , where  $P_{\text{in}} = 2\pi/\Omega(r_{\text{in}})$  is the rotation period at the innermost disk radius. In Figures 8 and 9, the spiral like shapes of different iso-level contours plotted on the  $xy$ -plane reveal the similar nonaxisymmetric nature of these modes. In the long run, such as for  $t > 100P_{\text{in}}$ , the surface density perturbations of both axisymmetric and nonaxisymmetric modes grow in amplitude only for  $r \lesssim 2r_{\text{in}}$  within the same domain. We illustrate this typical behavior in Figure 11 as compared to Figure 10 for the case of axisymmetric mode with frequency  $\kappa$ . Note that the perturbations at the time  $t = 15P_{\text{in}}$  (see Fig. 10) are comparable in amplitude over the whole computational domain ( $r_{\text{in}} \leq r \leq 3r_{\text{in}}$ ). The perturbations at the time  $t = 200P_{\text{in}}$ , however, have large amplitudes only for  $r_{\text{in}} \leq r < 2r_{\text{in}}$  whereas their amplitudes become negligible for  $r \gtrsim 2r_{\text{in}}$  (see Fig. 11).

In the global three-dimensional magnetohydrodynamic simulations of black hole accretion disks, the innermost disk region near the ISCO was found to show QPOs with frequency around the maximum of epicyclic frequency (Machida & Matsumoto 2003). In one of the recent simulations of the three-dimensional magnetohydrodynamic accretion flows around Schwarzschild black holes (Kato 2004), the structure of the flow has been changed at radial distances within the  $3.8r_{\text{S}} \leq r \leq 6.3r_{\text{S}}$  range, where  $r_{\text{S}}$  is the Schwarzschild radius. Two pairs of QPOs have been observed to be excited in that region with frequencies around the Keplerian frequency and the sum of Keplerian and epicyclic frequencies in the power spectra of these simulations. Most importantly, the frequency ratio of these QPO features has been found to be near 1.5. These results are in close agreement with the result of our mode analysis in the present work.

## 5. DISCUSSION AND CONCLUSIONS

We have probed the stability of the global modes in the inner region of a standard accretion disk around a black hole. Our study is the application of the recently developed analysis of global hydrodynamic modes (see EPA08) to the identification of the high-frequency QPO pairs observed in black hole sources. The presence of the ISCO allows for effects of strong gravity on both the dynamical frequencies and the global hydrodynamic parameters. Our pseudo-Newtonian approach takes account of these effects to determine the frequency bands and the growth rates of the unstable modes in the inner disk.

The disk is truncated at the radius of the ISCO,  $r_{\text{in}}$ . The growth rates of the modes are negative for sufficiently large distances from the ISCO. We find that the modes grow in am-

plitude only within a narrow zone in the innermost disk region. For a non-rotating black hole ( $a = 0$ ) the characteristic radii of the zone lie in the  $\simeq r_{\text{in}} - 2.1r_{\text{in}}$  range. The modes grow within the  $\simeq r_{\text{in}} - 2.5r_{\text{in}}$  range for a rotating black hole with spin  $a = 0.9$ . Among the growing modes the growth rates of the frequency branches around  $\Omega$  and 0 are higher as compared to those of the modes with frequency bands around  $\Omega \pm \kappa$  and  $\kappa$  (see Figs. 3–6). Due to the effect of enhanced hydrodynamic corrections on the growth rates, the modes grow faster in an accretion regime with relatively high rate and viscosity (see EPA08).

The radiation flux due to viscous energy dissipation in the inner disk takes the highest values within the narrow region where the modes grow (see Fig. 2). We deduce from the radial profiles of the mode frequencies that the frequency ratio of the modes around  $\Omega + \kappa$  and  $\Omega$  bands is very close to 1.5 at the radius where the disk radiation is maximum. This value was observed for the frequency ratio of the high-frequency QPO pairs in black hole sources (see Remillard & McClintock 2006). Instead of being excited at a particular radius in the disk, the hydrodynamic modes grow in a region of finite radial extension. To make an estimation for the expectation value of a frequency band and therefore for the frequency ratios of the relevant modes, we calculate the flux weighted averages of the frequency bands over the innermost disk region where the modes grow. Scanning the ratios of the expected mode frequencies for all possible values of the spin parameter  $a$  (see Fig. 7), we find that only the modes around  $\Omega + \kappa$  and  $\Omega$  branches have a frequency ratio around 1.5. This ratio is slightly higher than 1.5 if the black hole is a slow rotator ( $0 \leq a \lesssim 0.8$ ). The same ratio falls below 1.5 for fast rotating black holes ( $0.9 \lesssim a < 1$ ). The frequency ratios of other modes significantly deviate from 1.5 over a wide range of values for the spin parameter. Relying on the observed values for the frequency ratio of the upper high-frequency QPO to the lower one, we conclude that the modes with frequency branches  $\Omega + \kappa$  and  $\Omega$  are the most plausible candidates for the high-frequency QPOs from black holes.

The observations of high-frequency QPOs can be used to determine the underlying mechanism that produces these oscillations and to measure the spin parameter of the black hole (Remillard & McClintock 2006). Our analysis may provide a way to employ the observed frequency ratio of a high-frequency QPO pair in a given source to estimate the spin parameter  $a$ . In this sense, Figure 7 comes out as an efficient tool for reading the spin parameter  $a$  that corresponds to the value of  $\langle \Omega + \kappa \rangle / \langle \Omega \rangle$  to be interpreted as the frequency ratio of a high-frequency QPO pair observed in the X-ray power spectra of the black hole source.

There are several reasons for expecting to see the fingerprint of global long wavelength modes in the form of high-frequency QPOs observed in the X-ray power spectra of black hole sources in LMXBs. As compared to the neutron stars, there is little chance for accretion flows around the black holes in LMXBs to be affected by the dynamical action of a magnetic field of stellar origin. In the case of a black hole, instead of a direct feedback from the compact object, except gravity, the fluctuations in the mass transfer rate from the binary companion introduce perturbations with a broad band of frequencies including those of the inner disk. The disk modes which depend on global disk parameters become unstable in the innermost disk region and thus the disk oscillation frequencies are selectively amplified without any need for an

external mechanism to force them to attain high amplitudes. Furthermore, the observable luminosity variation in the X-ray light curve of a source due to global free oscillation modes of long wavelength, that is, of sufficiently large lengthscale is expected to be least affected by the MHD turbulent eddies of short wavelength. According to our present analysis, the higher the mass accretion rate  $\dot{M}$  and the greater the viscosity parameter  $\alpha$ , the higher are the growth rates of the modes. We therefore expect to observe these modes particularly in the state of high mass accretion rate and high viscosity. In such a state, the turbulent disk may also interact with its corona (see Tagger & Varnière 2006). This would lead to the formation of high-frequency QPOs in a spectral state where the contribution from the power law component is important. In our present analysis we identify the relevant disk modes without deliberating the disk-corona interaction which we plan to consider in a future work.

I would like to express my special thanks to M. A. Alpar who carefully read the manuscript and contributed it through various suggestions and to D. Psaltis for reading the manuscript and very useful discussions. I also thank U. Ertan for his valuable comments. I would like to thank the anonymous referee whose suggestions lead me to improve this manuscript. I acknowledge support from TÜBİTAK (The Scientific and Technical Research Council of Turkey) for a postdoctoral fellowship and the Marie Curie FP6 Transfer of Knowledge Project ASTRONS, MKTD-CT-2006-042722.

## REFERENCES

- Abramowicz, M. A., Karas, V., Kluźniak, W., Lee, W. H., & Rebusco, P. 2003, *PASJ*, 55, 467
- Alpar, M. A., Hasinger, G., Shaham, J., & Yancopoulos, S. 1992, *A&A*, 257, 627
- Alpar, M. A., & Psaltis, D. 2008, *MNRAS*, 391, 1472
- Alpar, M. A., & Yilmaz, A. 1997, *NewA*, 2, 225
- Beckwith, K., Hawley, J. F., & Krolik, J. H. 2008, *MNRAS*, 390, 21
- Belloni, T., Méndez, M., & Homan, J. 2005, *A&A*, 437, 209
- Chan, C., Psaltis, D., & Özel, F. 2009, *ApJ*, 700, 741
- Erkut, M. H., & Alpar, M. A. 2004, *ApJ*, 617, 461
- Erkut, M. H., Psaltis, D., & Alpar, M. A. 2008, *ApJ*, 687, 1220
- Kato, S. 2001, *PASJ*, 53, 1
- Kato, S., & Fukue, J. 1980, *PASJ*, 32, 377
- Kato, Y. 2004, *PASJ*, 56, 931
- Machida, M., & Matsumoto, R. 2003, *ApJ*, 585, 429
- Méndez, M., & Belloni, T. 2007, *MNRAS*, 381, 790
- Miyamoto, S., Kimura, K., Kitamoto, S., Dotani, T., & Ebisawa, K. 1991, *ApJ*, 383, 784
- Miyamoto, S., & Kitamoto, S. 1989, *Nature*, 342, 773
- Morgan, E. H., Remillard, R. A., & Greiner, J. 1997, *ApJ*, 482, 993
- Motch, C., Ricketts, M. J., Page, C. G., Ilavskiy, S. A., & Chevalier, C. 1983, *A&A*, 119, 171
- Mukhopadhyay, B., & Misra, R. 2003, *ApJ*, 582, 347
- Muno, M. P., Morgan, E. H., Remillard, R. A., et al. 2001, *ApJ*, 556, 515
- Novikov, I. D., & Thorne, K. S. 1973, in *Black Holes*, ed. C. DeWitt & B. S. DeWitt (New York: Gordon & Breach), 343
- Nowak, M. A., & Wagoner, R. V. 1991, *ApJ*, 378, 656
- Paczynski, B., & Wiita, P. J. 1980, *A&A*, 88, 23
- Page, D. N., & Thorne, K. S. 1974, *ApJ*, 191, 499
- Psaltis, D., Belloni, T., & van der Klis, M. 1999, *ApJ*, 520, 262
- Psaltis, D., & Norman, C. 2000, *arXiv:astro-ph/0001391*
- Remillard, R. A., & McClintock, J. E. 2006, *ARA&A*, 44, 49
- Remillard, R. A., Muno, M. P., McClintock, J. E., & Orosz, J. A. 2003, *BAAS*, 35, 648
- Remillard, R. A., Sobczak, G. J., Muno, M. P., & McClintock, J. E. 2002, *ApJ*, 564, 962
- Shakura, N. I., & Sunyaev, R. A. 1973, *A&A*, 24, 337
- Shapiro, S. L., & Teukolsky, S. A. 1983, in *Black Holes, White Dwarfs, and Neutron Stars* (New York: Wiley)

Sobczak, G. J., McClintock, J. E., & Remillard, R. A., et al. 2000, ApJ, 531, 537  
 Stella, L., Vietri, M., & Morsink, S. M. 1999, ApJ, 524, L63  
 Strohmayer, T. E. 2001, ApJ, 552, L49  
 Tagger, M., & Varnière, P. 2006, ApJ, 652, 1457

van der Klis, M. 1994, A&A, 283, 469  
 van der Klis, M. 2000, ARA&A, 38, 717  
 Wijnands, R., Homan, J., & van der Klis, M. 1999, ApJ, 526, L33  
 Wijnands, R., & van der Klis, M. 1999, ApJ, 514, 939

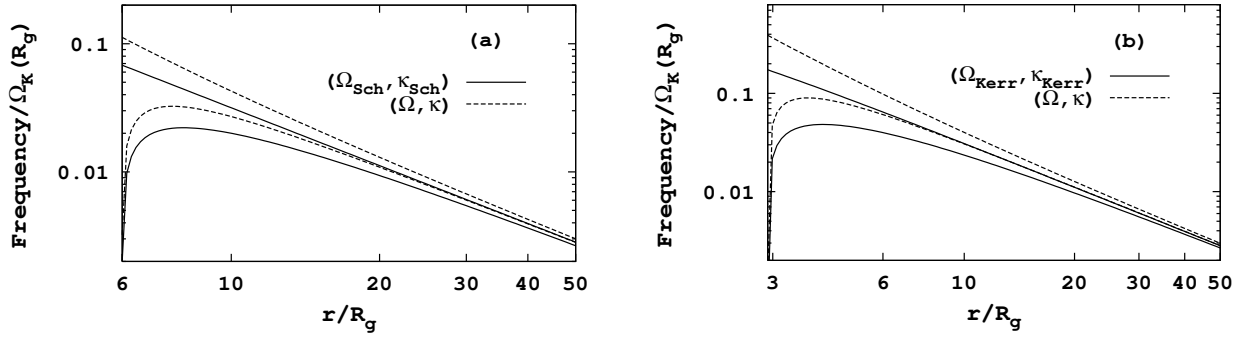


**Figure 1.** Radial profiles of the orbital and epicyclic frequencies. The Schwarzschild orbital and radial epicyclic frequencies  $\Omega_{\text{Sch}}$  and  $\kappa_{\text{Sch}}$  and the Kerr orbital and radial epicyclic frequencies  $\Omega_{\text{Kerr}}$  and  $\kappa_{\text{Kerr}}$  are shown by the solid curves. The pseudo-Newtonian orbital frequency  $\Omega$  and the pseudo-Newtonian radial epicyclic frequency  $\kappa$  are shown by the dashed curves. The panel (a) is obtained for a non-rotating black hole with spin parameter  $a = 0$ . The frequencies in panel (b) are plotted for a rotating black hole with spin parameter  $a = 0.8$ .

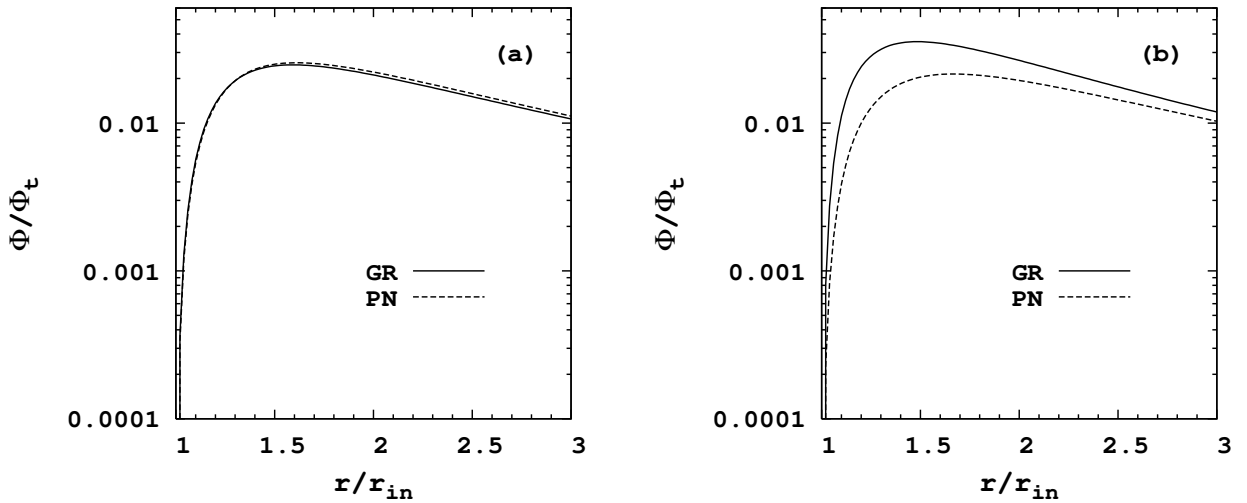


**Figure 2.** Radiation flux emerging from the inner disk. In both the panels (a) and (b), the solid curve represents the general relativistic (GR) estimation for the disk flux according to Page & Thorne (1974). The dashed curve in both the panels (a) and (b) estimates the disk flux according to our pseudo-Newtonian (PN) analysis. The panel (a) shows the flux from the accretion disk around a non-rotating black hole ( $a = 0$ ). The disk flux for a rotating black hole with spin parameter  $a = 0.9$  is displayed in panel (b).

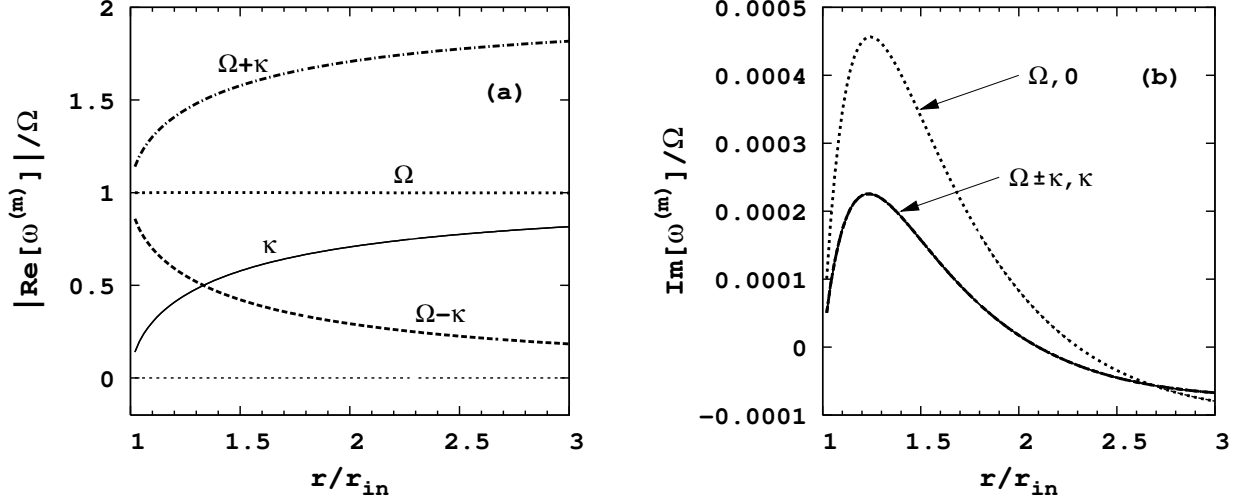


**Figure 3.** Real and imaginary parts of the complex frequencies for axisymmetric ( $m = 0$ ) and non-axisymmetric ( $m = 1$ ) modes in the innermost region of the accretion disk around a non-rotating black hole ( $a = 0$ ). The viscosity parameter and the accretion rate are  $\alpha = 0.1$  and  $\dot{m} = 0.1$ , respectively. The mode frequencies in panel (a) and the growth rates of the modes in panel (b) are labeled with the corresponding test-particle frequency branches.

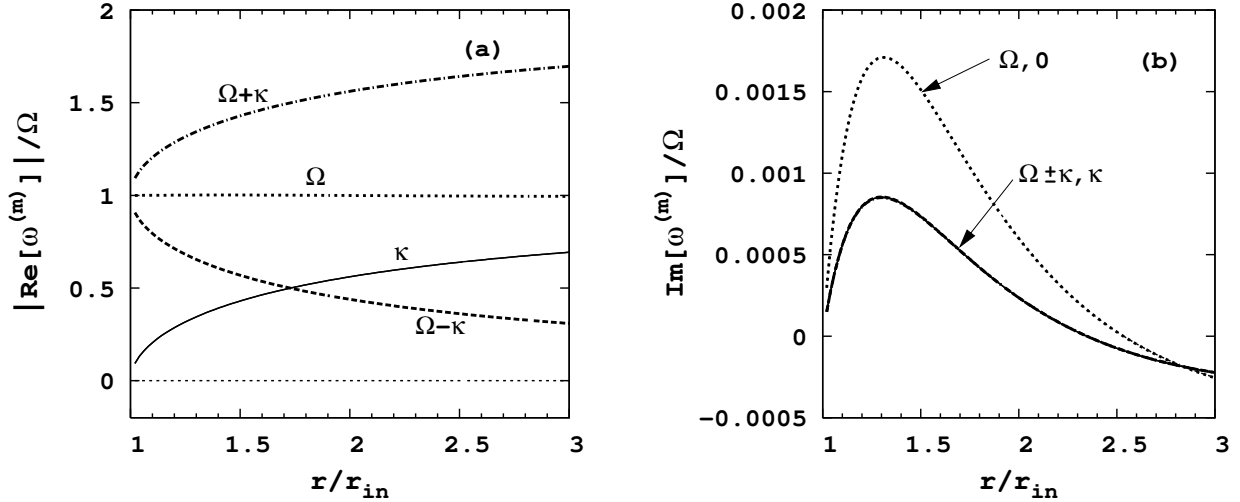


**Figure 4.** Real and imaginary parts of the complex frequencies for axisymmetric ( $m = 0$ ) and non-axisymmetric ( $m = 1$ ) modes in the innermost region of the accretion disk around a rotating black hole with spin parameter  $a = 0.9$ . The viscosity parameter and the accretion rate are  $\alpha = 0.1$  and  $\dot{m} = 0.1$ , respectively. The mode frequencies in panel (a) and the growth rates of the modes in panel (b) are labeled with the corresponding test-particle frequency branches.

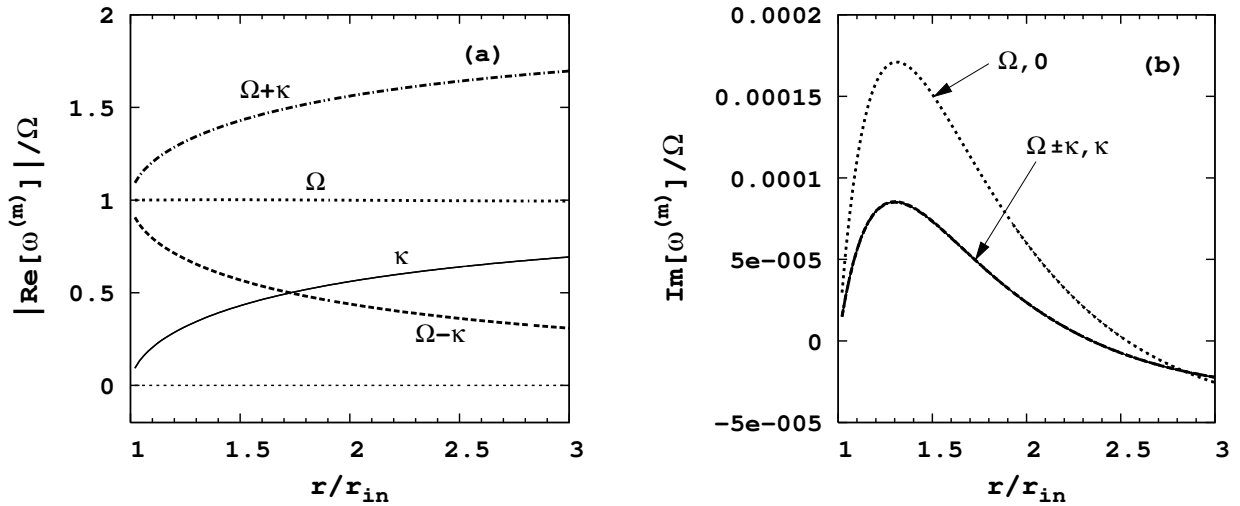


**Figure 5.** Real and imaginary parts of the complex frequencies for axisymmetric ( $m = 0$ ) and non-axisymmetric ( $m = 1$ ) modes in the innermost region of the accretion disk around a rotating black hole with spin parameter  $a = 0.9$ . The viscosity parameter and the accretion rate are  $\alpha = 0.01$  and  $\dot{m} = 0.1$ , respectively. The mode frequencies in panel (a) and the growth rates of the modes in panel (b) are labeled with the corresponding test-particle frequency branches.



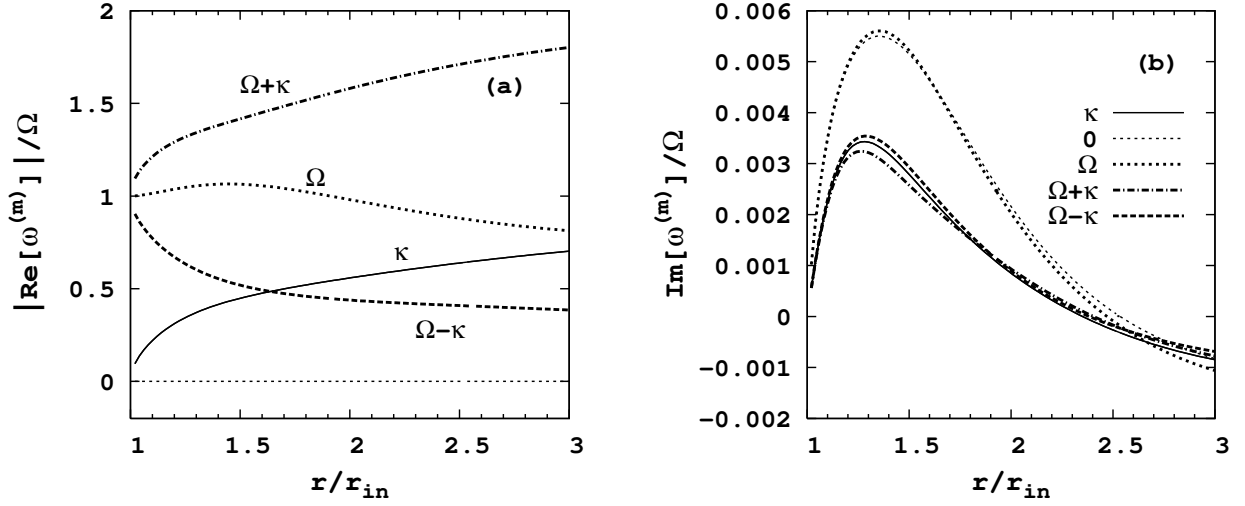


**Figure 6.** Real and imaginary parts of the complex frequencies for axisymmetric ( $m=0$ ) and non-axisymmetric ( $m=1$ ) modes in the innermost region of the accretion disk around a rotating black hole with spin parameter  $a = 0.9$ . The viscosity parameter and the accretion rate are  $\alpha = 0.01$  and  $\dot{m} = 0.6$ , respectively. The mode frequencies in panel (a) and the growth rates of the modes in panel (b) are labeled with the corresponding test-particle frequency branches.

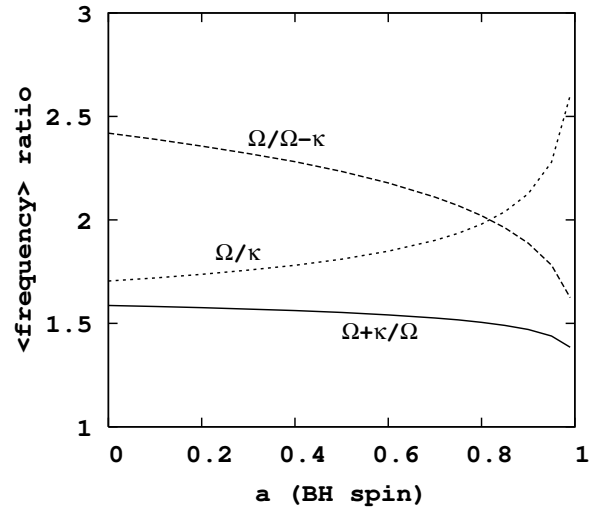


**Figure 7.** Ratios of the flux weighted averages of different frequency bands of the modes growing in the inner disk for all possible values of the spin parameter  $a$  between 0 and 1. The frequency ratios as functions of the spin parameter are obtained for the typical values,  $\alpha = 0.1$  and  $\dot{m} = 0.1$ .

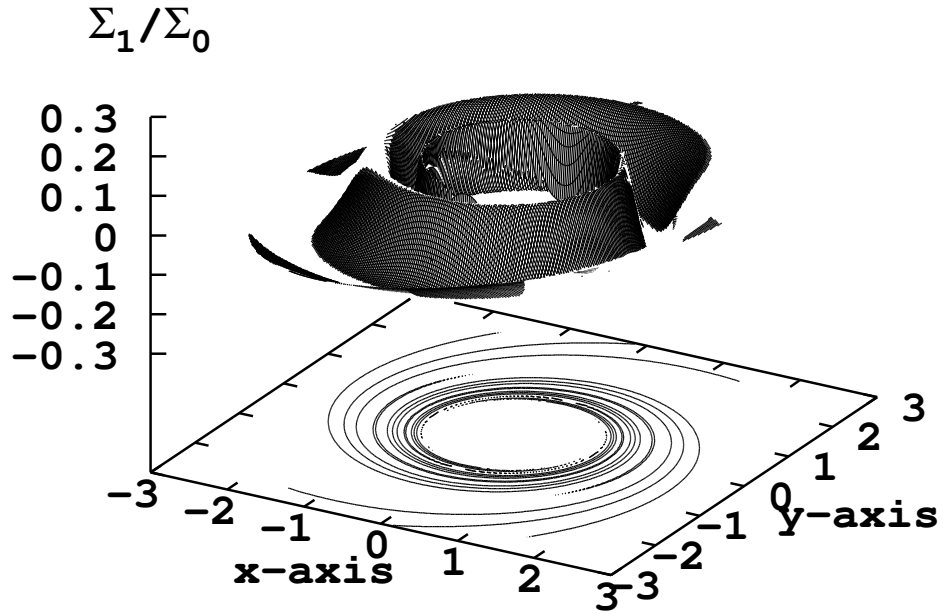


**Figure 8.** Profile of surface density perturbation  $\Sigma_1$  with respect to background surface density  $\Sigma_0$  for nonaxisymmetric mode with frequency  $\Omega$  in the innermost region ( $r_{\text{in}} \leq r \leq 3r_{\text{in}}$ ) of a disk around a rotating black hole with spin parameter  $a = 0.9$  for the typical values,  $\alpha = 0.1$  and  $\dot{m} = 0.1$ . The profile is obtained at the time  $t = 2P_{\text{in}}$ , where  $P_{\text{in}} = 2\pi/\Omega(r_{\text{in}})$  is the rotation period at the innermost disk radius.

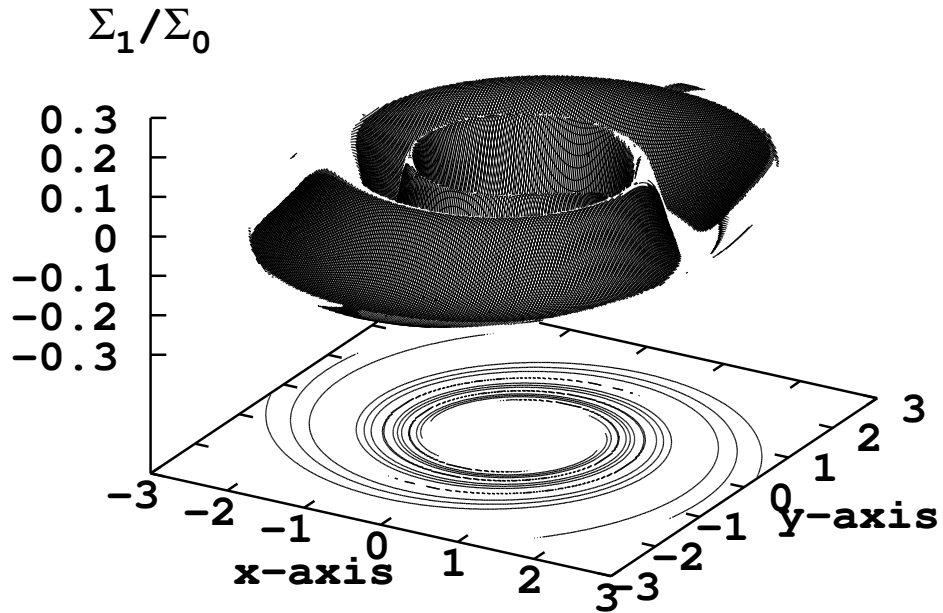


**Figure 9.** Profile of surface density perturbation  $\Sigma_1$  with respect to background surface density  $\Sigma_0$  for nonaxisymmetric mode with frequency  $\Omega + \kappa$  in the innermost region ( $r_{\text{in}} \leq r \leq 3r_{\text{in}}$ ) of a disk around a rotating black hole with spin parameter  $a = 0.9$  for the typical values,  $\alpha = 0.1$  and  $\dot{m} = 0.1$ . The profile is obtained at the time  $t = 2P_{\text{in}}$ , where  $P_{\text{in}} = 2\pi/\Omega(r_{\text{in}})$  is the rotation period at the innermost disk radius.

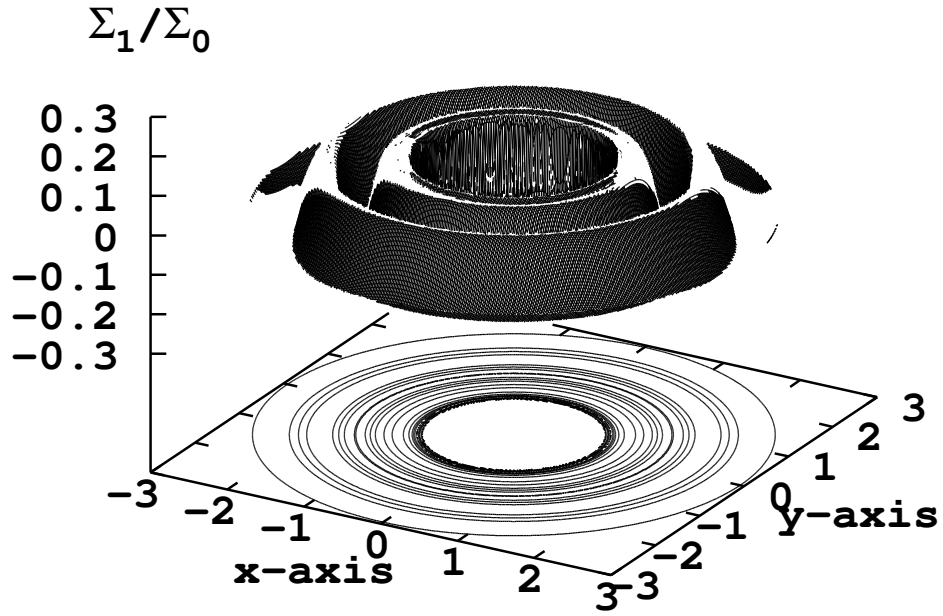


**Figure 10.** Profile of surface density perturbation  $\Sigma_1$  with respect to background surface density  $\Sigma_0$  for axisymmetric mode with frequency  $\kappa$  in the innermost region ( $r_{\text{in}} \leq r \leq 3r_{\text{in}}$ ) of a disk around a rotating black hole with spin parameter  $a = 0.9$  for the typical values,  $\alpha = 0.1$  and  $m = 0.1$ . The profile is obtained at the time  $t = 15P_{\text{in}}$ , where  $P_{\text{in}} = 2\pi/\Omega(r_{\text{in}})$  is the rotation period at the innermost disk radius.

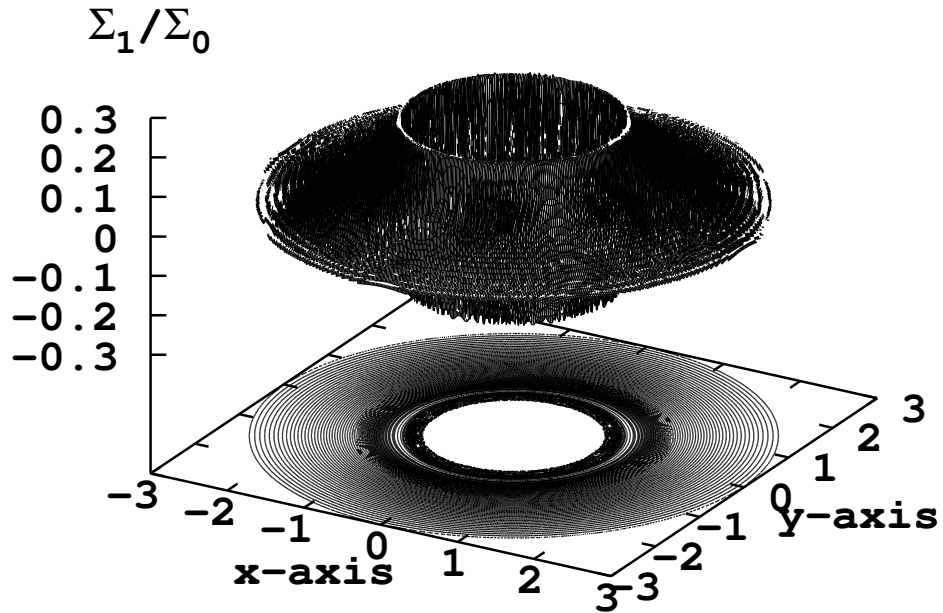


**Figure 11.** Profile of surface density perturbation  $\Sigma_1$  with respect to background surface density  $\Sigma_0$  for axisymmetric mode with frequency  $\kappa$  in the innermost region ( $r_{\text{in}} \leq r \leq 3r_{\text{in}}$ ) of a disk around a rotating black hole with spin parameter  $a = 0.9$  for the typical values,  $\alpha = 0.1$  and  $m = 0.1$ . The profile is obtained at the time  $t = 200P_{\text{in}}$ , where  $P_{\text{in}} = 2\pi/\Omega(r_{\text{in}})$  is the rotation period at the innermost disk radius.